Planar Micro-thermoelectric Generators Based on Cu55Ni45 and Ni90Cr10 Thermocouples for IoT Applications

Ibrahim Bel-Hadj, Zahia Bougrioua, K. Ziouche

Planar Micro-Thermoelectric Generators based on $Cu_{55}Ni_{45}$ and $Ni_{90}Cr_{10}$ Thermocouples for IoT applications

I. BEL-HADJ*, Z. BOUGRIOUA, AND K. ZIOUCHE

Univ. Lille, CNRS, Centrale Lille, Polytechnique Hauts-de-France, UMR 8520 - IEMN-Institut d'Electronique de Microélectronique et de Nanotechnologie, F-59000 Lille, France
*ibrahim.bel-hadj@univ-lille.fr, zahia.bougrioua@iemn.fr, katir.ziouche@univ-lille.fr

ABSTRACT

In this work, we present our novel planar micro-thermoelectric generators (µTEGs) integrating an original "folded" thermopile topology, periodically distributed on suspended membranes. The thermopile integrates eco-friendly and low-cost materials as Constantan ($Cu_{45}Ni_{55}$) and Chromel ($Ni_{90}Cr_{10}$) that build up thermocouples associated both in series and in parallel. This dual association allows to drastically reduce the thermopile electrical resistance (down to a few tens to a few hundred ohms) and so to electrically better adapt them. To optimize the structural dimensions of the µTEG, numerical simulations have been performed by 3D-finite element modeling using COMSOL Multiphysics© software. Several µTEG modules integrating this folded thermopile have been manufactured using Silicon micro-technologies that differ from our former expertise. In 3-membrane-based modules the harvested output power can reach 108 µW/cm² (for 1 W heat injected into the µTEG) with an output voltage up to few hundred of millivolts, which is enough to supply micro devices for IoT applications.

KEY WORDS

Energy harvesting; thermoelectrics; micro-generator; planar; Silicon technology; thermal modeling.

I. INTRODUCTION

Numerous technologies of the future such as smart-energy management (İcan and T. B. Çelik., 2021) but also smart-city development (A. Sampathkumar *et al.* 2020) will undoubtedly rely on the Internet of Things (IoT). Even though, applications of IoT are growing at a rate never seen before (IoT Analytics., 2022), these ones are delayed by the lack of energy solutions to supply them with no maintenance requirement as for instance the need of battery replacements. Thus, all innovative solutions contributing to improve the renewable production of energy are playing a strategic role and many of them consist to harvest energy from the direct environment to produce electricity and supply the IoT nodes (H. Sun *et al.* 2018). Due to the abundance of heat, micro ThermoElectric Generators (µTEGs) have become an actual promising solution. The active part of these devices is mainly made up of the association of a set of thermocouples (TCs) generally connected in series electrically and in parallel thermally (D. M. Rowe, 2006). Their working principle is based on the Seebeck effect (T. J. Seebeck, 1821) corresponding to the conversion of temperature gradients into electrical voltage.

The performances of µTEGs are generally related to the nature of TE materials but also to their geometrical structures that can be classified in two main categories: vertical or planar configurations (Fig 1). Vertical configurations provide more power and often use better performing TEs such as Bismuth and Antimony alloys (G. J. Snyder and E. S. Toberer., 2008). However, these materials are expensive to develop, incompatible with Silicon technologies and are highly toxic. Planar structures, generally using thin TE films, present the advantage of *allowing the thermal adaptation* of µTEGs to their environment due to their *high and adjustable thermal resistance* (Z. Yuan *et al.* 2015). This paper presents first results of such µTEGs that use a new thermopile topology made of $Ni_{90}Cr_{10}$ (Chromel) and $Cu_{55}Ni_{45}$ (Constantan) based TEs integrated in an original topology periodically folded and distributed on a multi-membrane template. Two configurations of the µTEG, with 2 and 3 membranes, are designed and modeled using COMSOL Multiphysics® software, and are afterward fabricated using CMOS-compatible Silicon technology. The fabricated modules were tested under calibrated heat flux to measure the Seebeck voltage and the output power for various heat input.

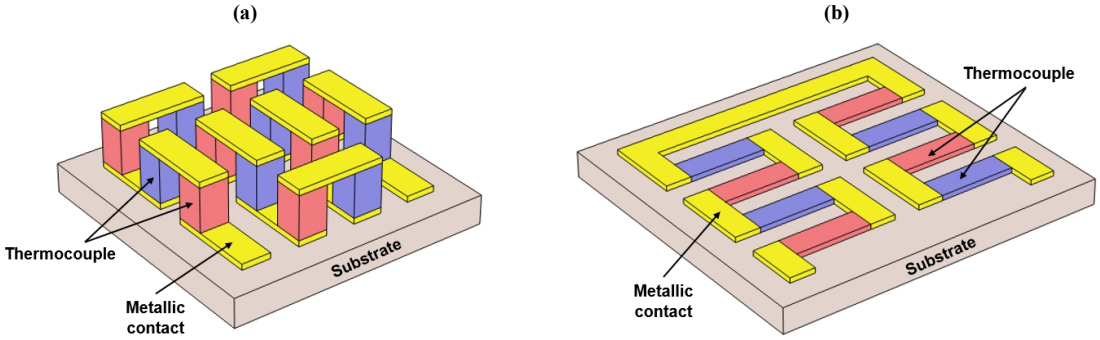

Fig. 1. The two typical µTEG structures: (a) vertical (π), (b) planar.

II. µTEG DESIGN

The structure of the planar µTEG proposed in this work (total area $\boldsymbol{A_{\mu TEG}}$ ~ 6 mm × 5.7 mm) is mainly composed of two parts (Fig 2) made up of two etched Silicon (Si) wafers:

• The first part (bottom part) is made of a set of membranes hollowed out and released in a Si substrate (380 µm thick (100) oriented Si). These periodically etched membranes are build up with a low-stress SiO_2/Si_xN_y bilayer, obtained by stress compensation of the two layers of 800 and 600 nm (M. Hafar, 2007) which limits bowing events and contribute to the mechanical strength of the whole structure. An innovative thermopile based on $Cu_{55}Ni_{45}$ and $Ni_{90}Cr_{10}$ TCs is designed with an original topology, "periodically folded", and distributes perpendicularly on the multi-membrane template. The details of the design and the fabrication steps of the thermopile were described in I. Bel-Hadj *et al*. (2022). Finally, a thick Polyimide layer (12 µm thick) is used for the passivation, electrical insulation of the thermopile and also contributes to the robustness of the membranes. For a given strip width of 200 µm (typical example), we count a quantity of TCs proportional to the number of membranes: $\mathbf{N_{TC} = 50 \times N_m}$ (taking into account

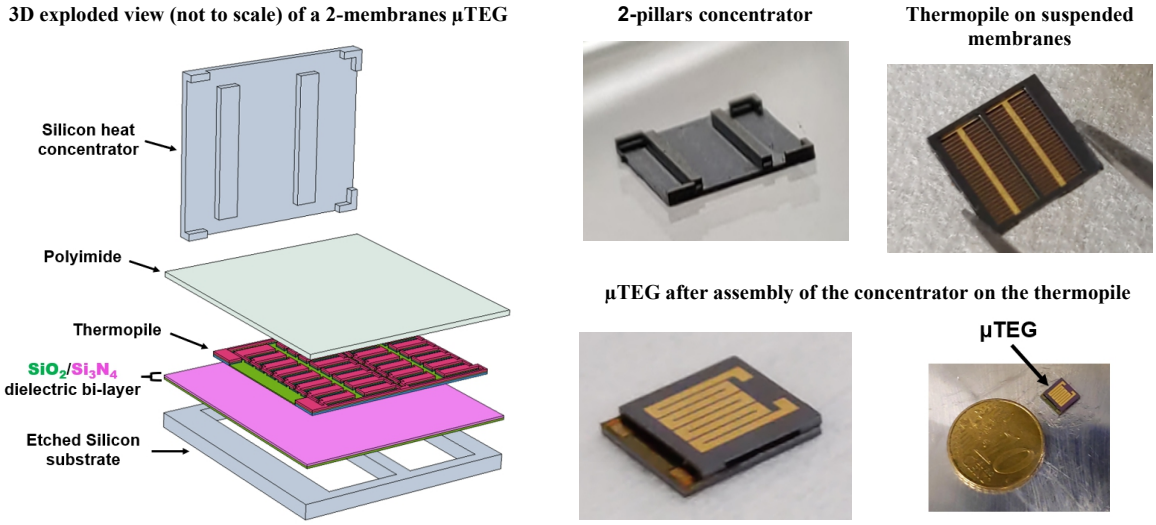

Fig. 2. Design of the novel µTEG.

the area used by the thermopile). The measured Seebeck coefficient of an elementary TC is about 48 µV/K.

• The second part of the module (top part) corresponds to a Silicon heat concentrator (top surface ~ 5.7 mm × 5.2 mm, 380 µm thick) made of a set of $\mathbf{N_m}$ pillars (230 µm thick, length ~ 5.1 mm, and width optimized according to number of pillars (I. Bel-Hadj *et al.* 2019). These allow to canalize the harvested heat flux, from the surface of the concentrator

down towards the heat sink, through the membranes (the pillar contacts with the membranes are located at the hot junction places of the thermopile). Four mechanical supports (bosses) located at the 4 corners of the concentrator are used to ensure a rigid support of the concentrator on the substrate and avoid the breaking of the membranes. So one part of the incident heat flux that is lost through the 4 bosses (i.e., without passing through the membranes): this part is directly proportional to the total contact surface between these bosses and the heat sink wafer. This contact surface must be as small as possible to minimize these lateral losses. But a compromise must be made in order not to weaken the µTEG too much (surface too small), experimentally, this surface was fixed at 1.2 mm^2.

The heat concentrator will be aligned on the suspended membranes such a way that the pillars are centered over the middle of the membranes. This is performed under optical microscopy using alignment wedges. Thermal grease is used to ensure a good wet contact between concentrator pillars and membranes and minimize thermal contact resistance.

III. RESULTS AND DESCUSSION

A. 3D THERMAL MODELING

To predict the temperature distributions across the µTEGs structures and the temperature gradients between the TC's junctions, the 3D structure of the µTEG is modeled using COMSOL Multiphysics® software, based on the finite element method. The description of the model and the simplifying computational assumptions as well as the boundary conditions on which the µTEG is submitted are detailed in I. Bel-Hadj *et al.* (2022). The symmetry of the structure allows to *model only half of the µTEG*, in order to reduce the calculation time and memory requirements.

The Fig 3 shows an illustration of the temperature distribution simulated for the half structures of µTEGs with 2 and 3 membranes. A heat flux density of 3.3 W/cm² is applied on the surface of the concentrator (surface ~ 0.3 cm²), corresponding to a net input heat of 1 W. A part of the input heat is lost by natural convection and radiation between the surface of the concentrator and the ambient environment. Another part is lost through the bosses. The temperature of the bottom surface of the heat sink is set at 25°C (equal to the ambient temperature). The heat flow through the $\mathbf{N_m}$ pillars of the concentrator, towards the membranes, creates periodic temperature gradients between the junctions of each TC constituting the thermopile, as shown in Fig 3. The simulation results corresponding to the applied boundary conditions, allow to calculate that the temperature differences generated between the hot and cold junctions $\Delta \boldsymbol{T_{hc}}$, are 137 K and 120 K and those between the surface of the concentrator and the heat sink $\Delta \mathbf{T_{ext}}$, are 142 K, 126 K, respectively for the 2 and 3-membranes µTEGs. The percentages of the fluxes exchanged by convection, radiation and that lost through the bosses are respectively of 11%, 5% and 37% for 2-membranes µTEG and of 9%, 4% and 33% for 3-membranes µTEG.

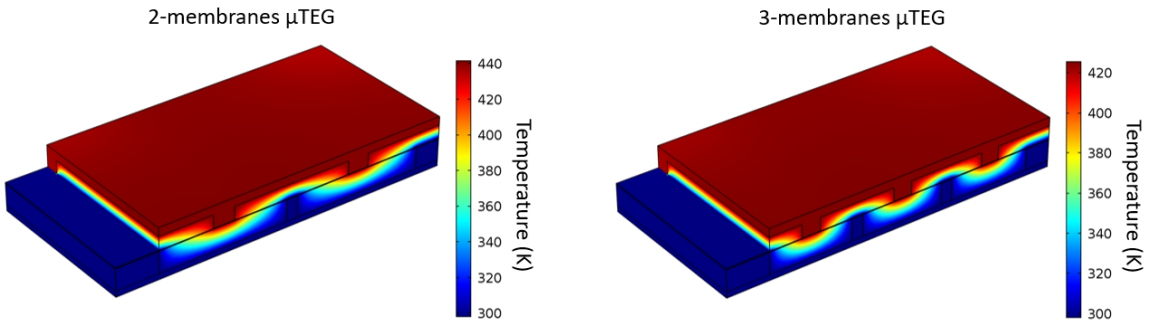

Fig. 3. Temperature distribution calculated for 2- and 3-membranes µTEGs. An input power of 1 W is injected into the concentrator and the temperature of the bottom side of the substrate is kept at 25 °C.

To optimize the structural dimensions of the µTEG, simulations have been carried out for modules integrating up to 10 membranes. These studies will be presented in an upcoming paper.

B. CHARACTERIZATION OF THE µTEGS

The two fabricated devices (2 and 3-membranes µTEGs) were tested using a four-probe set-up over a heat input range of 0 – 1.2W. The measurement principle consists in injecting a calibrated heat input by Joule effect in the heater (resistance in gold realized directly upon the surface of the concentrator as seen in Fig 2) with two probes, and measuring with the two other probes the Seebeck voltage generated from the device. The characteristics of the µTEG configurations realized and characterized in this work are presented in Tab 1. All these modules have an identical footprint ($A_{\mu TEG}$); the only difference is the number of thermocouples and membranes (and the number of concentrator pillars) depending of the length of the thermoelements. Concerning the thicknesses of TE materials, the both modules have 150 nm of $Ni_{90}Cr_{10}$ and 450 nm of $Cu_{55}Ni_{45}$.

µTEG	Number of membranes	Thermocouple lengths (µm)	Strip widths (µm)		Number of thermocouples	Internal electrical resistance (Ω)
			$Ni_{90}Cr_{10}$	$Cu_{55}Ni_{45}$		
2m-µTEG	2	1060	200	150	100	305
3m-µTEG	3	670	200	150	150	140

Tab. 1. Main parameters of the 2 fabricated and characterized µTEG configurations.

Each µTEG is characterized several times by adjusting the alignment between the concentrator and the bottom part of the module. The Fig 4 shows the best measured Seebeck ($\mathbf{V_S}$) voltage generated from the both devices as a function of the heat injected into the concentrator. $\mathbf{V_S}$ increases linearly with increasing heat input and reach a maximum of about 201.6 mV obtained by the µTEG with 2 membranes for a maximum injected heat input of 1.2 W. The linear characteristics of the Seebeck voltage as a function of the input power are naturally explained by Seebeck effect:

$$V_S = N_s \alpha_{TC} \Delta T_{hc} = N_s \alpha_{TC} R_i^{th} \phi_i$$

where N_s is the number of TCs connected in series fixed by the stripe width (N_s=25 for a stripe width of 200µm), $\alpha_{TC} = (\alpha_{NiCr} - \alpha_{CuNi})$ is the equivalent Seebeck coefficient of a TC, $\Delta T_{hc} = R_i^{th} \phi_i$ is the effective temperature difference between the hot and cold junctions, R_i^{th} is the internal thermal resistance of the µTEG, and ϕ_i is the input power injected into the concentrator. The dependence of the Seebeck voltage on the thermal resistance of the µTEG, which depends on the number of membranes (fixed by the length of the TCs, see Tab 1) explains the differences between the Seebeck voltages delivered by the both µTEG configurations.

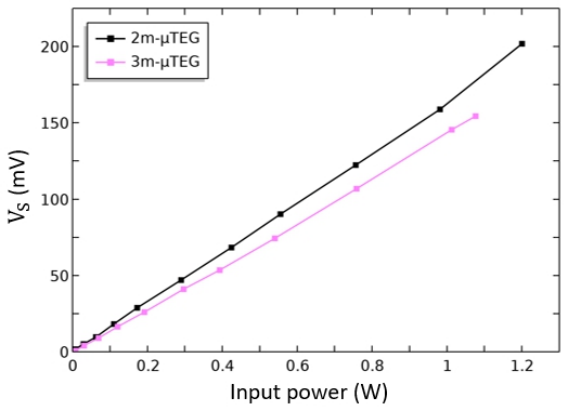

Fig. 4. Seebeck voltage generated by 2 and 3-membranes µTEGs versus input power injected into the concentrator.

The maximum output power density generated by the µTEG (corresponding to the power generated to a matched load resistance) can be calculated using the measured Seebeck voltage by:

$$P_{max} = \frac{V_S^2}{4R_{int}A_{\mu TEG}}$$

where R_{int} is the internal electrical resistance of the µTEG (305 Ω and 140 Ω respectively for 2 and 3 membranes µTEG). We note that the internal resistances of this new family of µTEGs with an all-metal thermopile, are clearly lower than those of the first generation modules, based on a periodically plated poly-Silicon thermopile, for whom R_{int} were of the order of a few hundred kΩ to a few MΩ for modules with 2 membranes (Z. Yuan *et al*. 2015).

Fig 5 shows the maximum output power density (P_{max}) generated by the µTEGs as a function of the input heat injected into the concentrator. The maximum generated output power density is about 125 µW/cm^2 for an injected input power of ~ 1.07 W obtained with 3-membranes µTEG. Normalized to 1W of injected input power, this is equivalent to the output power of 108.3 µW/cm². This corresponds to an efficiency factor (Strasser *et al*. 2004) defined by $P_{max}/\Delta T_{ext}^2$ (where ΔT_{ext} is the external temperature difference between the two heat sources in which the device is placed) of about 6.82 × 10^{-3} µW.cm^{-2}.K^{-2} when the ΔT_{ext} is about 126 K which correspond to 1W of heat injected into the concentrator. These performances are much better than of state-of-the-art modules using metallic thermoelectrics (for instance see Y. Shimizu *et al.* 2018 and B. Iezzi *et al.* 2017).

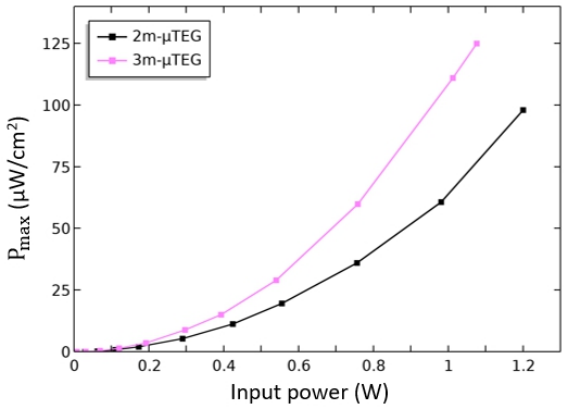

Fig. 5. Maximum output power density generated versus input power injected into the concentrator.

IV. CONCLUSION

In this study, we have presented a novel planar µTEG for thermal energy harvesting. The technology implemented is based on an original folded thermopile topology periodically distributed onto suspended membranes. The thermopile integrates metallic TE materials based on $Cu_{55}Ni_{45}$ and $Ni_{90}Cr_{10}$ that build up thermocouples associated both in series and in parallel. The use of metallic TE materials allowing to reduce the internal electrical resistance of the µTEGs compared to our first generation based on polysilicon thermopile. The fabrication of these devices is implemented using CMOS-compatible process of microfabrication. For 1 W heat injected into the heat concentrator, the maximum power is 108 µW/cm² with an efficiency factor of 6.82 × 10^{-3} µW.cm^{-2}.K^{-2} for µTEG configurations with 3 membranes. These first results will be followed by other studies to improve the performances of these µTEGs.

REFERENCES

[1]. Ö. İcan and T. B. Çelik, 2021. A Review on Smart Energy Management Systems in Microgrids Based on Power Generating and Environmental Costs. *In Applied Operations Research and Financial Modelling in Energy: Practical Applications and Implications, Cham: Springer International Publishing* (pp. 51-67).

[2]. A. Sampathkumar, S. Murugan, M. Sivaram, V. Sharma, K. Venkatachalam, and M. Kalimuthu, 2020. Advanced Energy Management System for Smart City Application Using the IoT. *In Internet of Things in Smart Technologies for Sustainable Urban Development*, *Cham: Springer International Publishing* (pp. 185-194).

[3]. IoT Analytics, 2022, May. State of IoT 2022: Number of connected IoT devices growing 18% to 14.4 billion globally. *https://iot-analytics.com/number-connected-iot-devices* (accessed Jun. 14, 2022).

[4]. H. Sun, M. Yin, W. Wei, J. Li, H. Wang, and X. Jin, 2018. MEMS based energy harvesting for the Internet of Things: a survey. *Microsyst Technol*, vol. 24, no. 7 (pp. 2853-2869).

[5]. D. M. Rowe, Ed., 2006. *Thermoelectrics handbook: macro to nano*. Boca Raton: CRC/Taylor & Francis.

[6]. T. J. Seebeck, 1821. Ueber den Magnetismus der galvanischen Kette. *Abh. K. Akad*. Wiss Berlin (pp. 290-346).

[7]. G. J. Snyder and E. S. Toberer, 2008, Feb. Complex thermoelectric materials. *Nature Mater*, vol. 7, no. 2 (pp. 105-114).

[8]. Z. Yuan, K. Ziouche, Z. Bougrioua, P. Lejeune, T. Lasri, and D. Leclercq, 2015. A planar micro thermoelectric generator with high thermal resistance. *Sensors and Actuators A: Physical*, vol. 221 (pp. 67-76).

[9]. M. Haffar, 2007, Étude et réalisation de matrices de microcapteurs infrarouges en technologie silicium pour imagerie basse résolution. *These de doctorat, Université de Lille. Available: https://www.theses.fr/2007LIL10053*.

[10]. I. Bel-Hadj, Z. Bougrioua, and K. Ziouche, 2022. Innovative 2.5D folded-thermopile for planar micro-thermoelectric generators. *Sensors and Actuators A: Physical*, Submitted.

[11]. I. Bel-Hadj, Z. Bougrioua, and K. Ziouche, 2019. Modélisation et optimisation de la structure géométrique d'un microgénérateur thermoélectrique planaire. *TELECOM'2019 & 11èmes JFMMA, 12-14 June 2019*, Saidia, Morocco. Available: https://hal.archives-ouvertes.fr/hal-02414487.

[12]. M. Strasser, R. Aigner, C. Lauterbach, T. F. Sturm, M. Franosch, and G. Wachutka, 2004, Sep. Micromachined CMOS thermoelectric generators as on-chip power supply. *Sensors and Actuators A: Physical*, vol. 114, no. 2-3 (pp. 362-370).

[13]. Y. Shimizu, M. Mizoshiri, M. Mikami, J. Sakurai, and S. Hata, 2018. Fabrication of Copper/Copper-Nickel thin-film thermoelectric generators with energy storage devices. *J. Phys. Conf. Ser., vol. 1052 (012032).*

[14]. B. Iezzi, K. Ankireddy, J. Twiddy, M. D. Losego, and J. S. Jur, 2017. Printed, metallic thermoelectric generators integrated with pipe insulation for powering wireless sensors. *Appl. Energy, vol. 208 (pp. 758–765).*